with three CH_2 groups, in contrast to the internal attack of another arene in which the most anchimerically assisted system is with one CH_2 unit. (See Table III.) Part of this

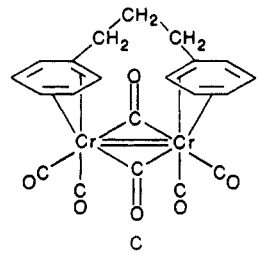

difference could be due to the preference for trans geometry in 1, as demonstrated by Reinke and Oehme.[8] However, it seems clear from the structure C that, if approximately octahedral geometry is maintained, the arene rings are held quite far apart by the bonds which are cis to both linear and bridged CO groups indicated in C. This requires a longer connecting chain.

Conclusions. We have demonstrated that both external and internal arene exchange in tricarbonylchromium complexes of bis(1,*n*-diarylalkanes) are catalyzed by nucleophiles and derive anchimeric assistance from the internal arene. We also show that the tricarbonylchromium group can catalyze arene exchange by neighboring group participation in bis(arene)tricarbonylchromium compounds.

Taken together, these results tend to confirm the general mechanism for arene exchange in which the bound arene progresses from η^6 to η^4 to η^2 bonding under the influence of attacking nucleophiles such as ketones, arenes, or (arene)tricarbonylchromium groups.

Acknowledgment. We are grateful to the National Science Foundation, Grant CHE84-20612, for support of this research.

Registry No. 1, 110434-23-6; 2, 108319-36-4; 3, 108319-37-5; 4, 109908-65-8; 5, 108319-38-6; 6, 82066-92-0; THF-d_8, 1693-74-9; acetone-d_6, 666-52-4; dioxane-d_8, 17647-74-4.

UV–PE Spectra and DV–Xα Calculations of Some Phosphido-Bridged Dimers

Gian Andrea Rizzi,[1a] Gaetano Granozzi,*[1a] Maurizio Casarin,[1b] and Marino Basato[1c]

Dipartimento di Chimica Inorganica, Metallorganica ed Analitica, Università di Padova, Padova, Italy, and Istituto di Chimica e Tecnologia dei Radioelementi del CNR and Centro di Studio sulla Stabilità e Reattività dei Composti di Coordinazione del CNR, Padova, Italy

Received April 23, 1987

Phosphido-bridged transition-metal complexes of the type $[(CO)_4M(\mu\text{-}PR_2)]_2$ (M = V, Cr, Mo, W, Mn) have been investigated by means of gas-phase ultraviolet (UV)–photoelectron (PE) spectroscopy and *first-principle* DV–Xα quantum mechanical calculations. The attention was focused on the variation of the metal–metal bond multiplicity along the series and on the changes in the whole electronic structure, with particular emphasis on the metal–bridge interactions. The increase in the metal–metal distance observed on going from the V to the Mn complex reflects the progressive occupation of antibonding metal–metal MOs. In agreement with such considerations, difference density maps for the V and Mn complexes show an evident charge accumulation between the two V atoms in contrast with a saddle point along the Mn–Mn axis. However, the large M–M lengthening observed on passing from Cr to Mn is more easily understood if the occupation of a M–bridge antibonding orbital is also taken into account. The UV–PE data and the theoretical results both demonstrate the existence of through-space interactions between the phosphorus bridging atoms, maximized in the Mn complex where the P–P distance takes the minimum value.

Introduction

Phosphido-bridged transition-metal complexes represent an interesting class of polynuclear compounds, in that they maintain their nuclearity in both substitution[2] and redox reactions,[3] so enabling, in principle, unusual reactivities via cooperative effect of the adjacent metals.[4] In this context, most of the very extensive studies has been mainly concerned so far with their synthesis and reactivity.[2,5]

The dinuclear-bridged complexes of the type $[(CO)_4M(\mu\text{-}PR_2)]_2$ were first prepared in the late 1964 by Chatt[6] and by Hayter.[7] On the basis of NMR studies, Hayter proposed a planar structure for the $M_2(\mu\text{-}PR_2)_2$ ring (see below) and this was later confirmed by several X-ray diffraction analyses which revealed centrosymmetrical structures.[8]

(1) (a) University of Padova. (b) ICTR CNR of Padova. (c) CSSRCC CNR of Padova.

(2) Basato, M. *J. Chem. Soc., Dalton Trans.* **1986**, 217 and references therein.

(3) (a) Madach, Th.; Vahrenkamp, H. *Chem. Ber.* **1981**, *114*, 513. (b) Trenkle, A.; Vahrenkamp, H. *J. Organomet. Chem.* **1982**, *236*, 71. (c) Dessy, R. E.; Kornmann, R.; Smith, C.; Haytor, R. *J. Am. Chem. Soc.* **1968**, *90*, 2001 and references therein.

(4) (a) Vahrenkamp, H. *Angew. Chem., Int. Ed. Engl.* **1978**, *17*, 379. (b) Johnson, B. F. G., Ed. *Transition Metal Clusters*; Wiley: New York, 1980. (c) Christholm, M. H.; Rothwell, I. P. *Prog. Inorg. Chem.* **1982**, *29*, 1. (d) Robert, D. A.; Geoffroy, G. L. In *Comprehensive Organometallic Chemistry*; Wilkinson, G., Stone, F. G. A., Abel, E., Eds.; Pergamon: London, 1982; Chapter 40. (e) Poilblanc, R. *Inorg. Chim. Acta* **1982**, *62*, 75. (f) Muetterties, E. L.; Kruse, M. J. *Angew. Chem., Int. Ed. Engl.* **1983**, *22*, 135.

(5) (a) Carty, A. J. *Adv. Chem. Ser.* **1982**, *No. 196*, 163. (b) Kreter, P. E.; Meek, D. W. *Inorg. Chem.* **1983**, *22*, 319. (c) Finke, R. B.; Gaughan, G.; Pierpont, C.; Cass, M. E. *J. Am. Chem. Soc.* **1981**, *103*, 1394. (d) Huttner, G.; Schneider, J.; Muller, H. D.; Mohr, G.; von Seyerl, J.; Wolfhart, L. *Angew. Chem., Int. Ed. Engl.* **1979**, *18*, 76. (e) Geoffroy, G. L.; Rosenberg, S.; Shulman, P. M.; Whittle, R. R. *J. Am. Chem. Soc.* **1984**, *106*, 1519. (f) Shyu, S. G.; Wojcicki, A. *Organometallics* **1984**, *3*, 809. (g) Regragui, R.; Dixneuf, P. H.; Taylor, N. J.; Carty, A. J. *Ibid.* p 814. (h) Wojcicki, A. *Inorg. Chim. Acta* **1985**, *100*, 125.

(6) (a) Chatt, J.; Thornton, D. A. *J. Chem. Soc.* **1964**, *1005*. (b) Chatt, J.; Thompson, D. T. *J. Chem. Soc.* **1964**, 2713.

(7) (a) Hayter, R. G. *Inorg. Chem.* **1964**, *3*, 711. (b) Hayter, R. G. *J. Am. Chem. Soc.* **1964**, *86*, 823.

0276-7333/87/2306-2536$01.50/0

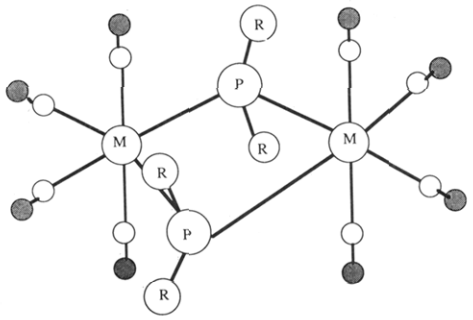

In 1978 Vahrenkamp[9] has structurally characterized the series of complexes with M = V, Cr, or Mn, and the very large differences in the observed M–M distances (V, 2.733 Å; Cr, 2.905 Å; Mn, 3.675 Å) were interpreted as a consequence of a strong variation in the metal–metal direct interactions. Actually, a simple application of the EAN rule, assuming the PR_2 ligand as mononegative, gives rise to the d^4–d^4, d^5–d^5, and d^6–d^6 electron count for V, Cr, and Mn complexes, respectively, so implying a metal–metal bond multiplicity of 2, 1, and 0 in the three cases. Successive EHT molecular orbital (MO) calculations by Shaik et al.[10] have confirmed such a view, since the following electronic configurations with respect with the M–M interactions were obtained: V, $\pi^2\delta^2\sigma^2\delta^{*2}$; Cr, $\pi^2\delta^{*2}\delta^2\sigma^2\pi^{*2}$; Mn, $\delta^{*2}\pi^2\delta^2\pi^{*2}\sigma^2\sigma^{*2}$. Fenske–Hall calculations on Cr and Mn dimers of this series also have been reported.[11]

A very efficient approach to study the interactions present in organometallic polynuclear molecules is the complementary use of the gas-phase ultraviolet–photoelectron (UV–PE) spectroscopy and an accurate MO theoretical method.[12] Actually, the experimental technique allows us to map the energy of the outermost occupied MOs and to test the results of the theoretical calculations which, on their own, furnish information on the bonding scheme. The DV–Xα method, adopted in the present work, is particularly efficient for this purpose since it is capable of describing accurately both the ground-state electronic structure and the energetics of the ionization process.

In this paper we report the results of an application of such methodological approach to the series of complexes $[(CO)_4M(\mu\text{-}PR_2)]_2$ (M = V, Cr, Mo, W, Mn; R = C_2H_5). Our attention was focused on the variation of the metal–metal bond multiplicity along the series and on the changes in the whole electronic structure, with particular emphasis on the metal–bridge interactions.

Experimental Section

Synthesis. The samples of $[(CO)_4M(\mu\text{-}PEt_2)]_2$ were synthesized according to the published procedures for the dimethylphosphido (V, Cr, Mo, W)[7,9] or diphenylphosphido (Mn)[7] analogues. After crystallization, their purity was checked by IR and NMR measurements.

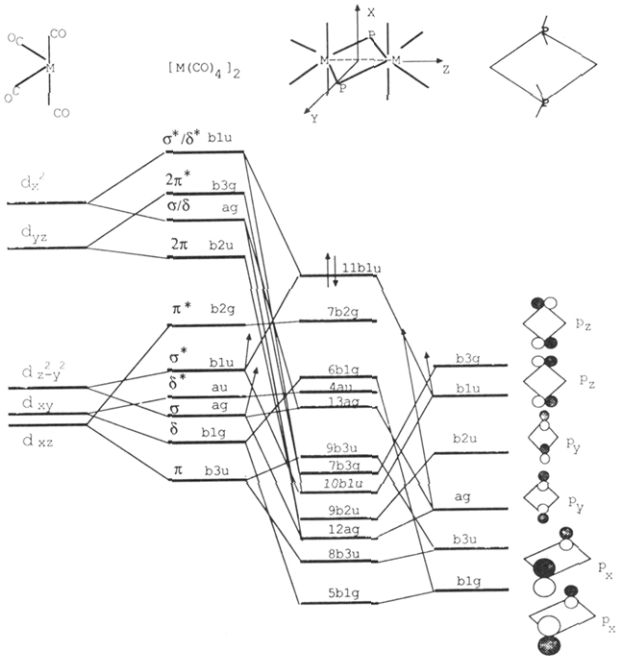

Figure 1. Qualitative correlation diagram between the orbitals of the constitutive fragments of $[(CO)_4M(\mu\text{-}PR_2)]_2$ complexes. Adopted axis system is also shown.

Spectra. He I and He II excited PE spectra were measured on a Perkin-Elmer PS-18 spectrometer modified for He II measurements by inclusion of a hollow cathode discharge lamp giving high output of He II photons (Helectros Developments). The ionization energy (IE) scale was calibrated by reference to peaks due to admitted inert gases (Xe–Ar) and to the He $1s^{-1}$ self-ionization. A heated inlet probe system was adopted at the following temperatures: 93 °C for Cr, 98 °C for Mo, 129 °C for W, and 99° for Mn complexes. Under the experimental condition in the ionization chamber the vanadium complex decomposes evoling CO, and any attempt to record its PE spectrum was unsuccessful.

Calculations. Hartree–Fock–Slater (HFS) discrete variational (DV–Xα) calculations[13] were performed on a VAX 8600 computer. Numerical atomic orbitals obtained for the neutral atoms (through 4p for V, Cr, Mn, 5p for Mo, 2p for C and O, and 3p for P) were used as basis functions. Due to the size of the investigated systems, orbitals 1s–3p (V, Cr, Mn), 1s–4p (Mo), 1s–2p (P), and 1s (C,O) were treated as frozen core in the molecular calculations. The molecular electronic density was approximated with an s-wave expansion, and the HFS equations were solved by a self-consistent charge (SCC) procedure[14] using the Gaspar–Kohn–Sham value[15] for the exchange scaling parameter. Atomic orbital populations were computed by using the Mulliken's population analysis.[16] To evaluate the magnitude of electronic relaxation associated with the removal of one electron from the various ground-state MOs, IE calculations were carried out by using Slater's transition-state formalism (TSIE).[17] The calculations have been carried out on model complexes where the bridge ethyl groups have been replaced by methyls. Their geometries (D_{2h}) have been obtained from the solid-state structural determinations[8,9] (see Figure 1 for the adopted axis system).

Results and Discussion

To have a better understanding of the DV–Xα results that will be soon discussed, it is useful to give a preliminar

(8) (a) Link, M. H.; Nassimbeni, L. R. *Inorg. Nuclear Chem. Lett.* **1973**, *9*, 1105. (b) Mais, R. H. B.; Owston, P. G.; Thompson, D. T. *J. Chem. Soc. A* **1967**, 1735.
(9) Vahrenkamp, H. *Chem. Ber.* **1978**, *111*, 3472.
(10) Shaik, S.; Hoffmann, R.; Fisel, R. L.; Summerville, R. H. *J. Am. Chem. Soc.* **1980**, *102*, 4555.
(11) Teo, B. K.; Hall, M. B.; Fenske, R. F.; Dahl, L. F. *J. Organomet. Chem.* **1974**, *70*, 413.
(12) For recent applications to the field of polinuclear molecules see: (a) Casarin, M.; Ajò, D.; Lentz, D.; Bertoncello, R.; Granozzi, G. *Inorg. Chem.* **1987**, *26*, 465. (b) Pilloni, G.; Zecchin, S.; Casarin, M.; Granozzi, G. *Organometallics* **1987**, *6*, 597. (c) Bertoncello, R.; Granozzi, G.; Cârsky, P.; Wiest, R.; Bénard, M. *J. Chem. Soc., Dalton Trans.* **1986**, 2581. (d) Casarin, M.; Ajò, D.; Vittadini, A.; Granozzi, G.; Bertoncello, R.; Osella, D. *Inorg. Chem.* **1986**, *25*, 511.
(13) Averill, F. W.; Ellis, D. E. *J. Chem. Phys.* **1973**, *59*, 6412.
(14) Rosen, A.; Ellis, D. E.; Adachi, H.; Averill, F. W. *J. Chem. Phys.* **1976**, *65*, 3629 and references therein.
(15) (a) Gaspar, R. *Acta Phys. Acad. Sci. Hung.* **1954**, *3*, 263. (b) Kohn, W.; Sham, L. J. *Phys. Rev.* **1965**, *140*, A1133.
(16) Mulliken, R. S. *J. Chem. Phys.* **1955**, *23*, 1833.
(17) Slater, J. C. *Quantum Theory of Molecules and Solids. The Self-Consistent Field For Molecules and Solids*; McGraw-Hill: New York, 1974, Vol. 4.

Table I. DV-Xα Results for $[(CO)_4V(\mu\text{-}P(CH_3)_2)]_2$

		% pop.							
		2V							
MO	$-\epsilon$, eV	s	p	d	2P	8CO	4C	12H	character
$7b_{2g}$(LUMO)	5.30	0	0	56	0	44	0	0	π^*(V–V)
$6b_{1g}$(HOMO)	6.07	0	0	49	0	36	15	0	δ(V–V)
$4a_u$	6.14	0	0	57	0	43	0	0	δ^*(V–V)
$13a_g$	6.51	0	0	65	0	26	8	1	σ(V–V)
$9b_{3u}$	6.65	0	0	56	1	29	14	0	π(V–V)
$7b_{3g}$	7.54	0	1	20	44	14	8	13	V–P
$10b_{1u}$	7.65	0	9	18	28	33	4	8	V–P
$9b_{2u}$	8.75	0	1	3	34	4	44	14	P–C
$12a_g$	9.28	0	6	8	32	6	36	12	P–C
$8b_{3u}$	9.34	0	0	4	31	12	40	13	P–C
$5b_{1g}$	9.48	0	0	3	34	9	40	14	P–C
$6b_{2g}$	10.94	0	0	0	0	72	19	9	C–O
$3a_u$	11.01	0	0	0	0	18	55	27	C–H
$7b_{3u}$	11.04	0	1	0	0	98	1	0	C–O

Table II. DV-Xα Results for $[(CO)_4Cr(\mu\text{-}P(CH_3)_2)]_2$

		% pop.							
		2Cr							
MO	$-\epsilon$, eV	s	p	d	2P	8CO	4C	12H	character
$11b_{1u}$(LUMO)	3.72	1	1	42	26	25	0	5	σ^*(Cr–Cr)
$7b_{2g}$(HOMO)	6.01	0	0	67	0	33	0	0	π^*(Cr–Cr)
$6b_{1g}$	6.35	0	0	58	0	30	12	0	δ(Cr–Cr)
$4a_u$	6.41	0	0	66	0	34	0	0	δ^*(Cr–Cr)
$13a_g$	6.62	0	0	69	3	24	4	0	σ(Cr–Cr)
$9b_{3u}$	6.86	0	0	59	0	33	8	0	π(Cr–Cr)
$7b_{3g}$	7.54	0	5	19	50	12	4	10	Cr–P
$10b_{1u}$	7.61	0	6	25	30	30	2	7	Cr–P
$9b_{2u}$	9.20	0	3	4	48	10	27	8	P–C
$8b_{3u}$	9.22	0	0	2	32	9	48	9	P–C
$5b_{1g}$	9.37	0	0	2	34	5	48	11	P–C
$12a_g$	9.88	0	5	5	40	20	23	7	P–C
$7b_{3u}$	10.39	0	0	0	0	81	11	8	C–O
$6b_{2g}$	10.41	0	0	0	0	100	0	0	C–O
$4b_{1g}$	10.55	0	0	0	2	53	30	15	

qualitative description of the interactions between the ligands and the metal atoms. A correlation diagram reporting the building up of the $[(CO)_4M(\mu\text{-}PR_2)]_2$ complex starting from the $M(CO)_4$ and the $(PR_2)_2$ fragments is pictured in Figure 1.

The frontier orbitals of the $M(CO)_4$ fragment are well-known:[18] a set of three inner orbitals (d_{xz},d_{xy} and $d_{z^2-y^2}$ in the adopted axis system, Figure 1), descended from the octahedral t_{2g} set (hereafter t_{2g}-like), and two outer hybrid orbitals ($p_z d_{x^2}$ and $p_y d_{yz}$) which are related to the octahedral e_g set (hereafter e_g-like). We can remember that the t_{2g}-like MOs have a back-bonding d$\rightarrow\pi^*$(CO) character while the e_g-like ones are M–CO σ antibonding and directed toward the bridging ligands of the dimeric complex. When two $M(CO)_4$ fragments (each accommodating four, five, or six electrons in the V, Cr, or Mn complexes, respectively) are allowed to interact,[10] M–M bonding and antibonding MOs are formed according to the scheme reported in Figure 1.[19] We must recall, however, that the energy ordering and splittings reported in Figure 1 are purely indicative since they will depend critically on the actual metal–metal distance, which changes along the series of the studied complexes.

The frontier orbitals of the $(PR_2)_2$ fragment are pictured in Figure 1. The phosphorus p_x (b_{3u} and b_{1g}) and p_y (a_g and b_{2u}) combinations lie lower in energy since they are mainly engaged into the P–R bonding and, consequently, they are used only to a limited extent for the M–bridge interaction. On the contrary, the high-lying p_z combinations (b_{3g} and b_{1u}) interact efficiently with empty e_g-like orbitals of the $M_2(CO)_8$ fragment, giving rise to M–P bonding orbitals. However, the b_{1u} orbital of the bridging fragment mixes also with a b_{1u} orbital of the t_{2g} like set ($d_{z^2-y^2}$) of the $M_2(CO)_8$ fragment. As a consequence, the usual three-orbital mixing mode is expected, i.e. a low-lying M–P bonding, an intermediate nonbonding, and a high-lying antibonding MOs.

DV-Xα eigenvalues and percentage population analysis of the outermost occupied MOs and of the LUMO of the model complexes $[(CO)_4M(\mu\text{-}P(CH_3)_2)]_2$ (M = V, Cr, Mn) are reported in Tables I–III. A diagram summarizing the trend of the orbital energies of the three complexes is pictured in Figure 2. The assignment of the dominant character of each MO was obtained according to symmetry considerations (with the help of the correlation diagram previously discussed) and by analyzing the relative contour plots (CPs), the most interesting ones being reported in Figure 3–6.

The following discussion of the theoretical results will be divided in two sections: in the first we will consider the metal–metal interaction while in the second the interaction between the phosphido bridge and the metal atoms will be analyzed.

Metal–Metal Bonding. Our theoretical results on the V(I), Cr(I), and Mn(I) complexes are in ageement with the 18-electron rule. The computed electronic configurations with respect to the metal–metal interactions are similar, but with a different ordering, to that obtained by the EHT

(18) Elian, M.; Hoffmann, R. *Inorg. Chem.* **1975**, *14*, 1058.

(19) As already pointed out in ref 10, the a_g and b_{1u} MOs do not represent pure σ M–M interactions but they have some δ character as well. This fact has been emphasized in Figure 1 for e_g-like a_g and b_{1u} MOs, where such a mixing is not negligible.

Table III. DV-Xα Results for $[(CO)_4Mn(\mu\text{-}P(CH_3)_2)]_2$

		% pop.							
		2Mn							
MO	−ϵ, eV	s	p	d	2P	8CO	4C	12H	character
$10b_{2u}$(LUMO)	3.49	0	10	18	11	58	3	0	Mn–P antibonding
$11b_{1u}$(HOMO)	6.40	1	0	72	4	23	0	0	σ*(Mn–Mn)
$13a_g$	6.53	0	6	58	0	32	4	0	σ(Mn–Mn)
$6b_{1g}$	6.75	0	0	58	1	33	8	0	δ(Mn–Mn)
$9b_{3u}$	6.78	0	0	56	1	32	10	1	π(Mn–Mn)
$7b_{2g}$	6.82	0	0	67	0	33	0	0	π*(Mn–Mn)
$4a_u$	6.92	0	0	63	0	37	0	0	δ*(Mn–Mn)
$10b_{1u}$	7.87	0	11	6	46	24	4	9	Mn–P
$9b_{2u}$	8.08	0	6	8	49	5	26	6	P–C
$7b_{3g}$	8.18	0	7	17	46	14	6	10	Mn–P
$5b_{1g}$	9.09	0	0	2	37	5	48	8	P–C
$8b_{3u}$	9.22	0	0	4	35	12	40	9	P–C
$12a_g$	10.26	0	1	3	40	13	34	9	P–C
$6b_{2g}$	10.54	0	1	0	0	96	2	1	C–O
$7b_{3u}$	10.57	0	1	0	0	91	5	3	C–O
$4b_{1g}$	10.65	0	0	0	1	68	20	11	

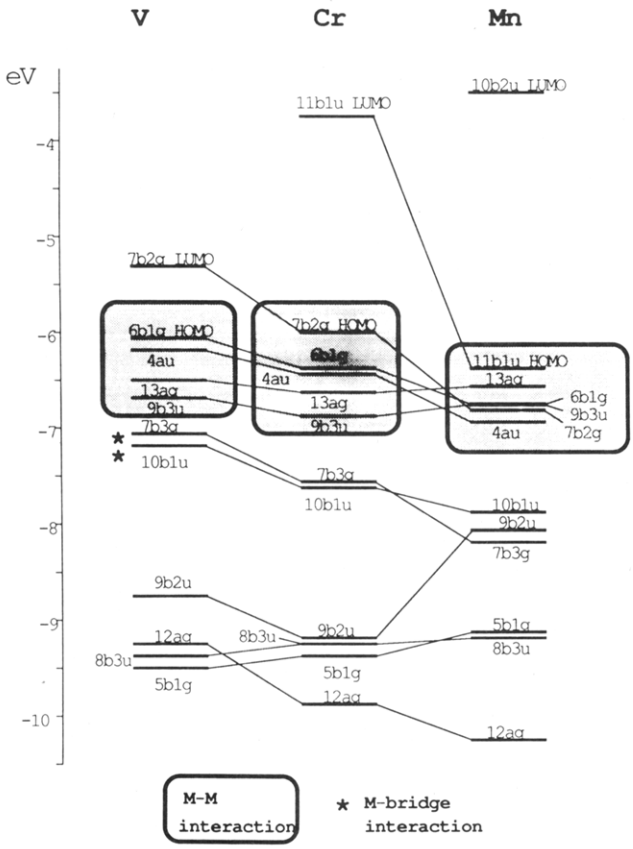

Figure 2. DV-Xα correlation diagram between one-electron energy levels of $[(CO)_4M(\mu\text{-}P(CH_3)_2)]_2$ complexes (M = V, Cr, Mn).

method:[10] V, $\pi^2\sigma^2\delta^{*2}\delta^2$; Cr, $\pi^2\sigma^2\delta^{*2}\delta^2\pi^{*2}$; Mn, $\delta^{*2}\pi^{*2}\pi^2\delta^2\sigma^2\sigma^{*2}$. It is confirmed, then, that the large increase in the metal–metal distance observed on going from the V to the Mn complex reflects the progressive occupation of antibonding metal–metal MOs.

Looking at the energy trend of the MOs involved into the metal–metal interactions along the V → Cr → Mn series (Figure 2), it is evident that only minor variations are present between the V and Cr complexes, whereas a large rearrangement of these MOs is observed in the Mn complex, where the six MOs involved in the M–M interactions span over a very narrow energy range. This trend parallels the structural changes observed by the X-ray diffraction studies:[8,9] i.e. a small M–M bond length increase on going from V to Cr (ca. 0.18 Å) and a much larger one from Cr to Mn (0.77 Å). In our opinion, the interpretation of such a behavior requires further discussion: on passing from V to Cr, a π*(M–M) MO ($7b_{2g}$) is occupied, which, by symmetry constraints, has no localization on the bridges. In contrast, the σ*(M–M) MO ($11b_{1u}$) of the Mn dimer is filled. It is important to point out, however, that in the Cr complex the $11b_{1u}$ LUMO has also M–P antibonding character due to negative overlap between the $d_{z^2-y^2}$ combinations and the bridge p_z orbitals (see the schematic picture below and the CP reported in Figure 3a).[20]

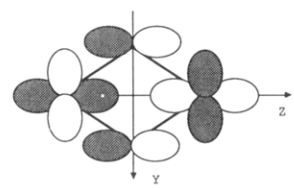

Therefore, besides the obvious larger effect on the M–M distance of a σ*(M–M) vs a π*(M–M) occupation, we propose a second factor concurring to the very large Mn–Mn observed distance. Actually, this M–P antibonding interaction is partially relieved by lengthening the M–M distance, as it is evidenced by (i) looking at the reduction of the localization of the $11b_{1u}$ MO on the P atoms on passing from Cr to Mn complex (compare Tables II and III), (ii) comparing the corresponding CPs (Figure 3a,b), and (iii) observing the very pronounced stabilization of the $11b_{1u}$ MO on passing from Cr to Mn (Figure 2).

An interesting consequence of the very large Mn–Mn bond distance is that all the MOs involved into the M–M interactions are practically nonbonding (see, for example, the comparison between $13a_g$ σ(M–M) MOs of Cr and Mn in Figure 4). The very narrow energy range of d orbitals of the Mn complex is then explained, in agreement with relative UV–PE data (see below). The nonbonding character of the d orbitals in Mn enhances their tendency to back-donate into 2π* orbitals of the CO ligands. This is monitored by two experimental and theoretical results: (i) the final theoretical metal gross atomic charge is higher in the Mn than in the Cr complex (Cr, +0.63 e; Mn, +1.03 e); (ii) the value of activation enthalpy for CO dissociation, in decalin, is higher for Mn (ΔH^* = 165 kJ mol^{-1})[21] than for Cr(ΔH^* = 125 kJ mol^{-1}).[22]

(20) The e_g-like d_{z^2} orbital is not significantly involved into the $11b_{1u}$ MO.

(21) Basato, M., unpublished results.

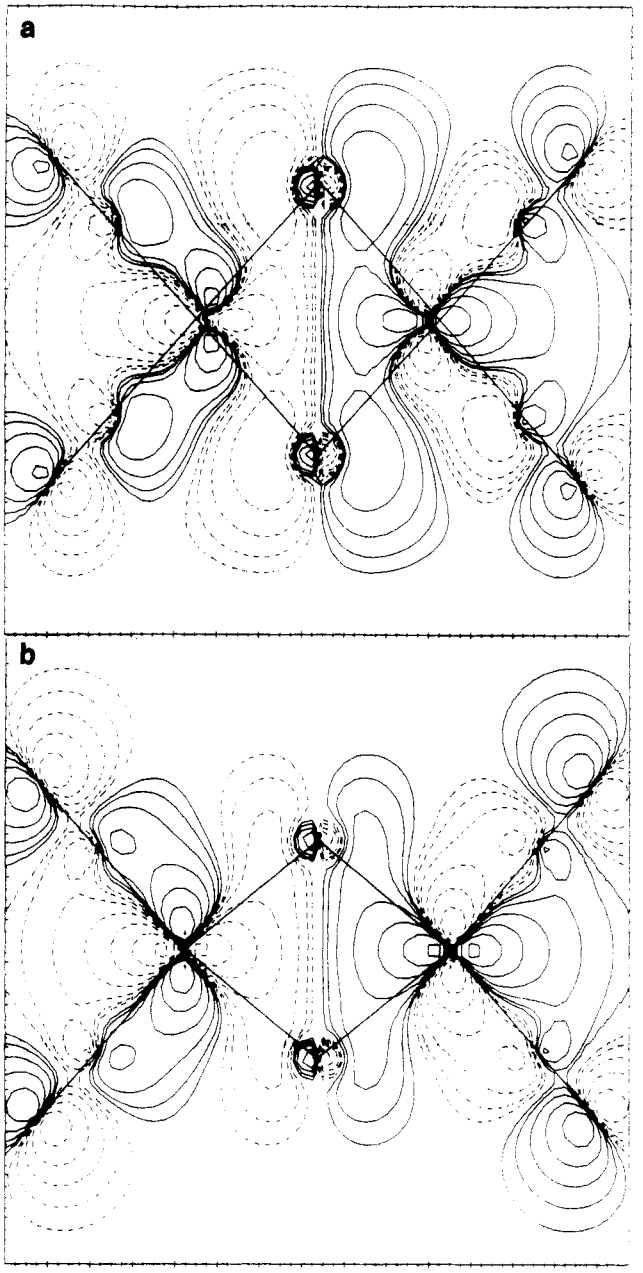

Figure 3. DV-Xα contour plots for $11b_{1u}$ MO of $[(CO)_4M(\mu\text{-}P(CH_3)_2)]_2$ complexes in the yz plane: (a) M = Cr; (b) M = Mn. Contour values are ±0.0065, ± 0.013, ±0.026, ±0.052, ±0.104, ±0.208, and ±0.416, ±0.832 $e^{1/2}/Å^{3/2}$ with negative values in dashed lines.

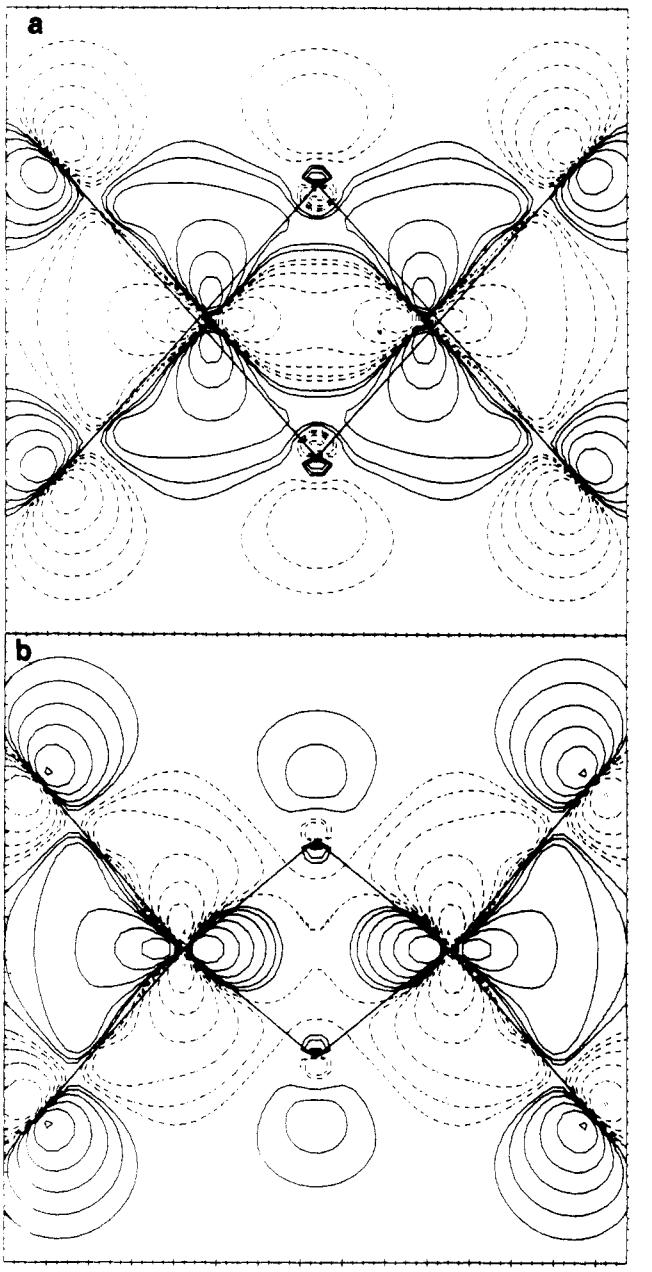

Figure 4. DV-Xα contour plots for $13a_g$ MO of $[(CO)_4M(\mu\text{-}P(CH_3)_2)]_2$ complexes in the yz plane: (a) M = Cr; (b) M = Mn. Plot parameters are identical with those of Figure 3.

Further comments are necessary to understand the counterintuitive energy ordering of the b_{1g} δ(M–M) and a_u δ^*(M–M) MOs: in all three complexes examined here the δ(M–M) component is always destabilized with respect to the δ^*(M–M) one. This can be understood by simple symmetry considerations: as shown in Figure 1, the δ(M–M)–δ^*(M–M) energy gap in the $[M(CO)_4]_2$ fragment is small because of weak overlap; since only the δ bonding b_{1g} component can interact with an inner orbital of the bridging fragment, it turns out that the relative destabilization is sufficient to reverse the usual δ–δ^* sequence. A similar counterintuitive ordering is found in the Mn dimer as to the π and π^* components: in this case the large metal–metal distance is responsible for quasi-degenerate π and π^* MOs (practically nonbonding) in $[M(CO)_4]_2$ so that a reversing of the π–π^* ordering is eventually obtained by the interaction of the b_{3u} π MO with the bridging fragment.

As a final consideration on the metal–metal bonding, we compare in Figure 7 the three-dimensional difference density maps in the yz plane for the V and Mn complexes. In agreement with considerations so far reported, there is an evident charge accumulation between the two V atoms (Figure 7a). On the contrary, a saddle point is observed along the Mn–Mn axis (Figure 7b).

Metal–Bridge Bonding. As already shown in Figure 1, the M–bridge bond is mostly described by the $7b_{3g}$ and $10b_{1u}$ MOs (Tables I–III, Figures 2 and 5). They originate from the p_z phosphorus orbitals which strongly overlap with the d_{yz} and $d_{z^2-y^2}$ metal orbitals. The involvement of the metallic d_{x^2} combinations into the $10b_{1u}$ MO appears to be very limited. We must point out that, because of their origin in the $M_2(CO)_8$ fragment, the $7b_{3g}$ MO has also a π^*(M–M) character (Figure 5a) and the $10b_{1u}$ one has a σ^*(M–M) nature (Figure 5b).

(22) Basato, M. *J. Chem. Soc., Dalton Trans.* **1985**, 91.

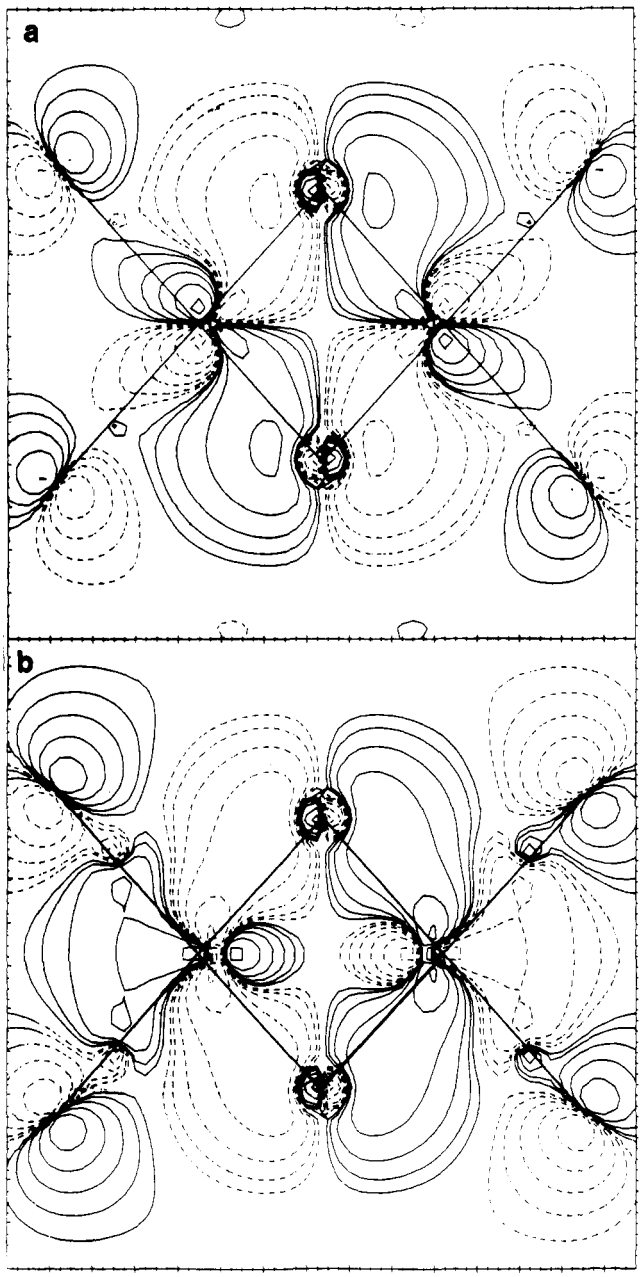

Figure 5. DV-Xα contour plots for (a) $7b_{3g}$ and (b) $10b_{1u}$ MOs of $[(CO)_4Cr(\mu\text{-}P(CH_3)_2)]_2$ in the yz plane. Plot parameters are identical with those of Figure 3.

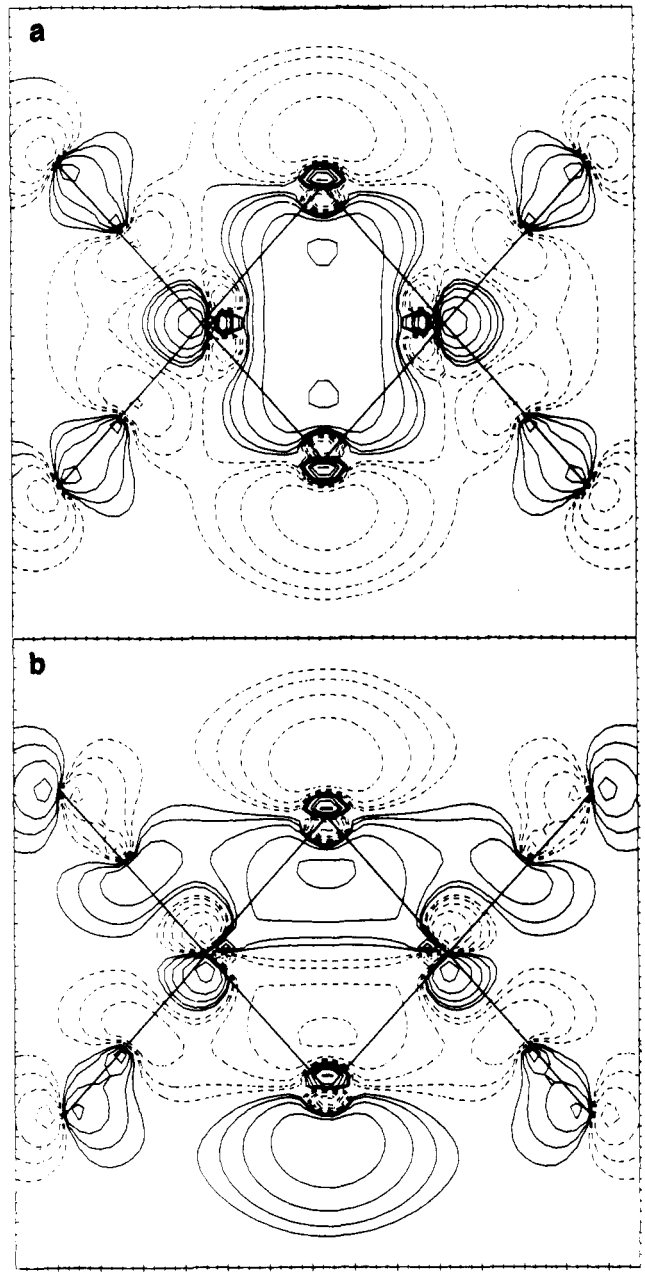

Figure 6. DV-Xα contour plots for (a) $12a_g$ and (b) $9b_{2u}$ MOs of $[(CO)_4Cr(\mu\text{-}P(CH_3)_2)]_2$ in the yz plane. Plot parameters are identical with those of Figure 3.

Both $7b_{3g}$ and $10b_{1u}$ MOs undergo an energy stabilization along the series V → Cr → Mn that can be explained both by energy matching and overlap considerations: (i) the larger M–M bond distances reduce the antibonding character of the b_{3g} and b_{1u} orbitals of the $[M(CO)_4]_2$ fragment, and the consequent energy stabilization gives rise to a better energy matching with the bridge partners; (ii) the change of geometry of the M_2P_2 ring (which is more elongated along the metal–metal axis in the Mn complex) gives rise to an increased overlap between the p_z phosphorus orbitals and the d metal orbitals on going from V → Cr → Mn. The latter effect is more marked for the $7b_{3g}$ MO than for the $10b_{1u}$ one, so that an energy inversion is observed in the Mn complex (see Figure 2).

The two MOs originating from p_y phosphorus orbitals ($9b_{2u}$ and $12a_g$, see Figure 6) show another interesting trend along the studied series. As expected, they are mainly engaged into the P–R bonds and only weakly involved in the M–P bond by a limited mixing with the $2\pi(b_{2u})$ and $\sigma(a_g)$ orbitals of the $[M(CO)_4]_2$ fragment. Their energy position is mainly dictated by the through-space interactions between the lobes of the p_y phosphorus orbitals pointing toward the center of the M_2P_2 ring (see Figure 1). Actually, the in-phase combination (a_g, Figure 6a) is always at lower energy than the out-of-phase one (b_{2u}, Figure 6b), and the energy splitting between them is dramatically increased (see Figure 2) in the Mn complex, where the P–P distance is shorter compared to those in the V and Cr cases (V, 3.84 Å; Cr, 3.62 Å; Mn, 2.92 Å).[8,9] Such an increase of the energy splitting finds a counterpart in the UV-PE spectra discussed later on.

Some interesting considerations can be also drawn from the comparison between the theoretical results of the two isoelectronic Cr and Mo complexes (see Figure 8). Whereas the metal–metal bonding scheme is virtually unchanged in the two cases (apart from a minor energy shift of all levels in the Mo complex), not negligible differences are theoretically predicted (and found in the UV-PE spectra, see below) for the M–bridge bonding and bridge-based orbitals. First, the $7b_{3g}$ MO, which in the Cr

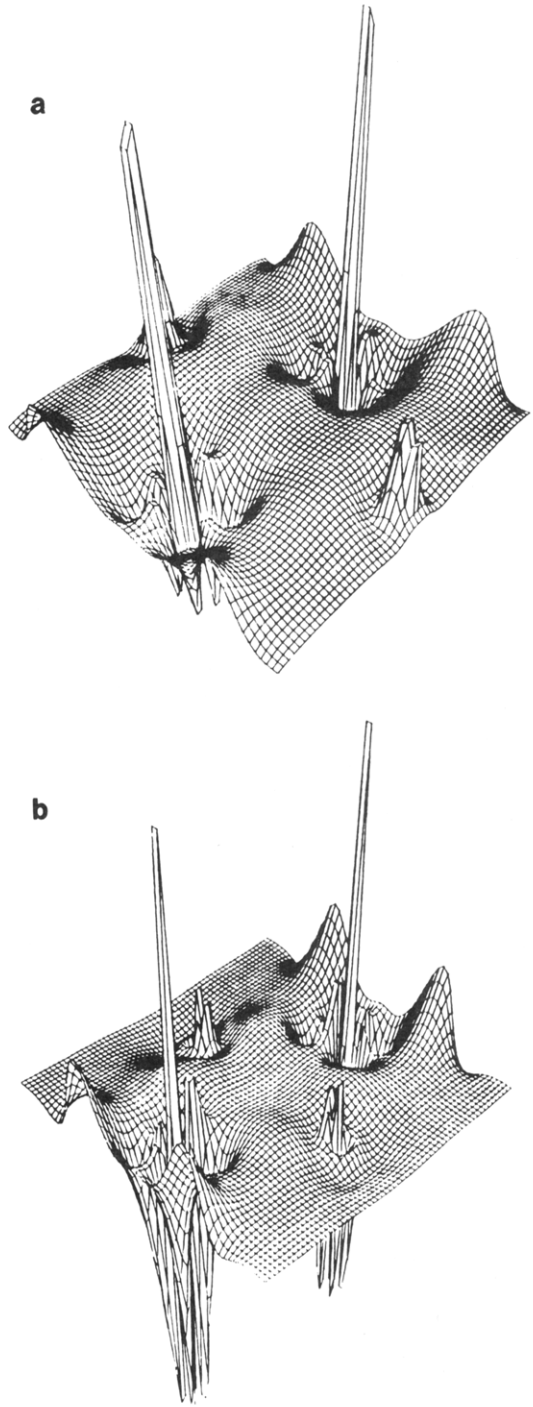

Figure 7. DV–Xα three-dimensional difference density maps in the *yz* plane for the $[(CO)_4M(\mu\text{-}P(CH_3)_2)]_2$ complexes: (a) M = V; (b) M = Mn.

complex has a strong Cr–P bonding character, is highly destabilized in Mo, leading to a smaller bonding Mo–P character. The main reason for that is certainly the worse energy matching between the metallic $2\pi^*$ orbital of the e_g-like set and the corresponding bridge-based orbital (see Figure 1) consequent to the larger t_{2g}–e_g splitting, typical of the second series transition metals. The second remarkable difference between Cr and Mo is related to the energy splitting between the p_y phosphorus-based orbitals ($12a_g$, $9b_{2u}$), which is much smaller in the heavier complex (Figure 8). Because of the larger Mo covalent radius, the Mo–P distance (2.50 Å)[8] is larger than the Cr–P one (2.32 Å),[9] and the P–P distance (3.96 Å) is increased, so reducing the above-mentioned through-space interaction.

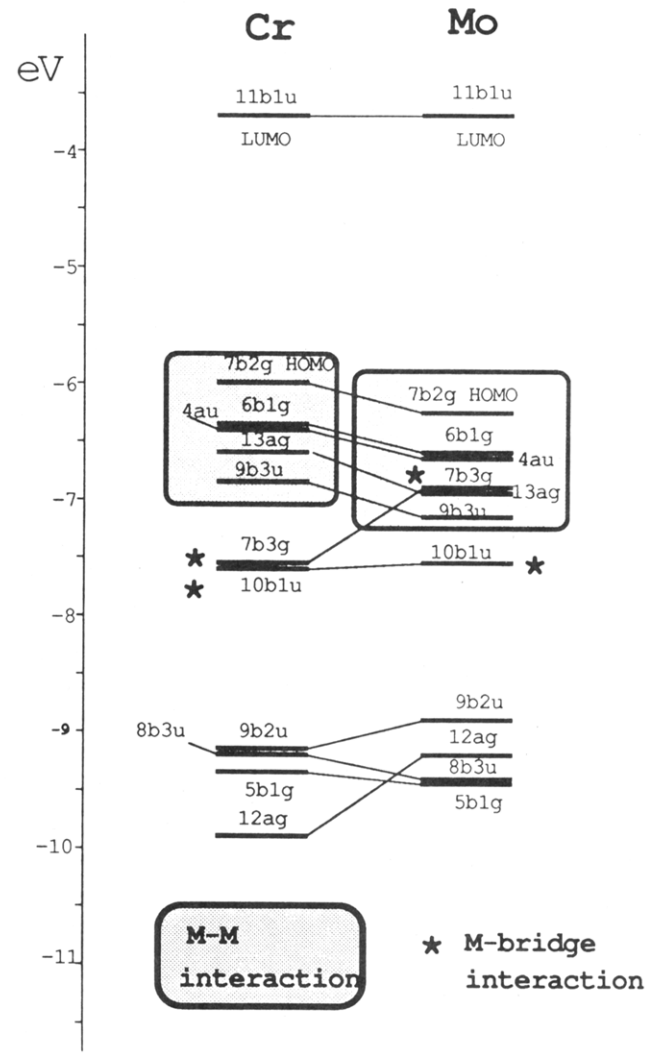

Figure 8. DV–Xα correlation diagram between one-electron energy levels of $[(CO)_4M(\mu\text{-}P(CH_3)_2)]_2$ complexes (M = Cr, Mo).

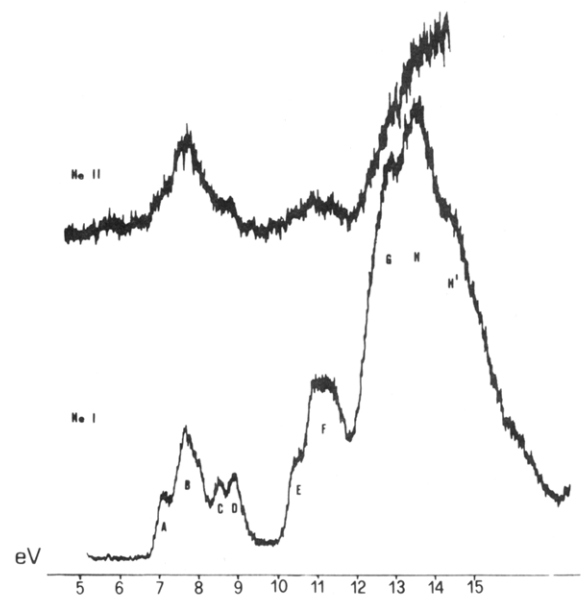

Figure 9. He I (bottom) and He II (top) excited PE spectra of $[(CO)_4Cr(\mu\text{-}P(C_2H_5)_2)]_2$.

UV–PE Spectra. The He I/He II excited PE spectra (up to 15 eV) of the $[(CO)_4M(\mu\text{-}PR_2)]_2$ (M = Cr, Mo, W, Mn; R = C_2H_5) complexes are reported in Figures 9–12, where bands have been alphabetically labeled. The vertical

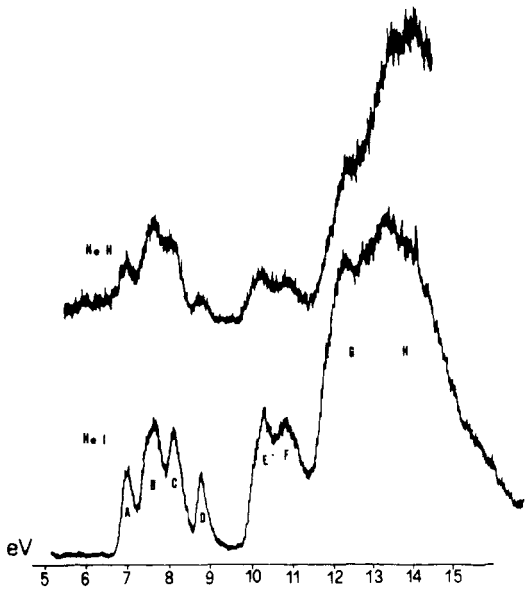

Figure 10. He I (bottom) and He II (top) excited PE spectra of $[(CO)_4Mo(\mu\text{-}P(C_2H_5)_2)]_2$.

Table IV. UV-PE Data[a,b] of $[(CO)_4M(\mu\text{-}P(C_2H_5)_2)]_2$ (M = Cr, Mo, W, Mn)

		Cr
A	7.09	$7b_{2g}$ (8.20)
B	7.68	[$6b_{1g}$ (8.50), $4a_u$ (8.64), $13a_g$ (8.84), $9b_{3u}$ (9.02)]
C	8.52	$7b_{3g}$ (9.70)
D	8.88	$10b_{1u}$ (9.73)
E	10.4	$9b_{2u}$ (11.13)[c]
F	10.9	[$8b_{3u}$ (11.20),[c] $5b_{1g}$ (11.27),[c] $12a_g$ (11.90)[c]]
G	12.9	
H	13.5	
H	14.6	
		Mo
A	7.03	$7b_{2g}$ (8.42)
B	7.67	[$6b_{1g}$ (8.72), $4a_u$ (8.78), $13a_g$ (9.10)]
C	8.11	$7b_{3g}$ (9.00), $9b_{31}$ (9.30)
D	8.79	$10b_{1u}$ (9.59)
E	10.30	$9b_{2u}$ (10.83),[c] $12a_g$ (11.20)[c]
F	10.84	$8b_{3u}$ (11.23),[c] $5b_{1g}$ (11.27)[c]
G	12.4	
H	13.4	
		W
A	7.01	$7b_{2g}$
B	7.79	[$6b_{1g}$, $4a_u$, $13a_g$]
C	8.29	$9b_{3u}$, $7b_{3g}$
D	9.02	$10b_{1u}$
E	10.6	$9b_{2u}$, $12a_g$
F	10.9	$8b_{3u}$, $5b_{1g}$
G	12.7	
H	13.4	
		Mn
A	7.29	$11b_{1u}$ (8.66)
B	8.1	[$13a_g$ (8.73), $9b_{3u}$ (8.88), $6b_{1g}$ (8.89), $7b_{2g}$ (9.03)]
C	8.6	$4a_u$ (9.12), $10b_{1u}$ (10.01)
D	9.4	$9b_{2u}$ (10.23), $7b_{3g}$ (10.26)[c]
E	10.89	[$5b_{1g}$ (11.00),[c] $8b_{3u}$ (11.15),[c] $12a_g$ (12.20)[c]]
F	12.2	
G	13.4	

[a] IEs reported are the mean values over several distinct runs. The extimated error is ±0.05 or ±0.1 eV according to the number of decimal places reported. [b] TSIEs reported in parentheses. [c] evaluated from TS procedure on HOMO.

IEs and the final assignments discussed hereafter are summarized in Table IV. Only the assignments of bands up to 12 eV will be discussed because the broad bands starting from 12 eV contain the body of the ionizations from the carbonyl framework and from the R substituents,

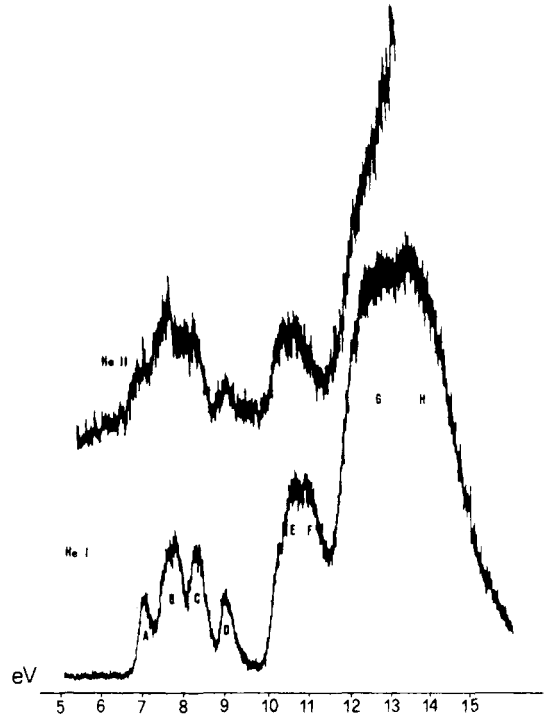

Figure 11. He I (bottom) and He II (top) excited PE spectra of $[(CO)_4W(\mu\text{-}P(C_2H_5)_2)]_2$.

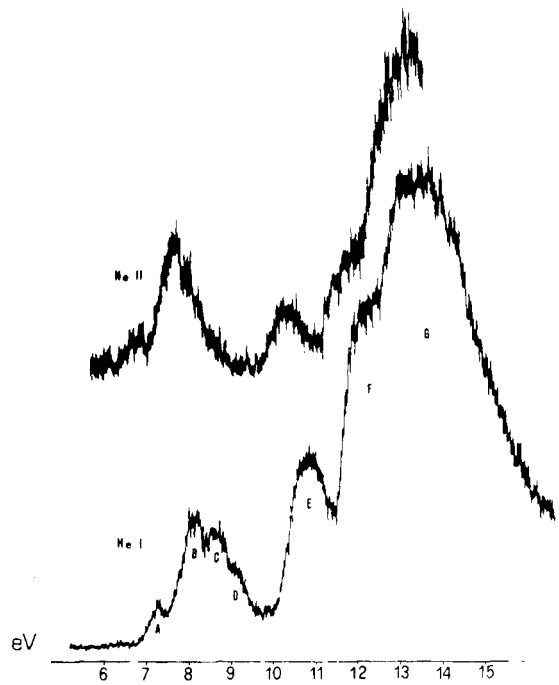

Figure 12. He I (bottom) and He II (top) excited PE spectra of $[(CO)_4Mn(\mu\text{-}P(C_2H_5)_2)]_2$.

whose consideration is out of the scope of this paper.

The assignments we propose are mainly based on the following criteria:[23] (i) comparison between the experimental IEs and theoretical TSIEs (Table IV);[24] (ii) relative intensity arguments between bands within each He I spectrum; (iii) changes in the relative intensity of the bands

(23) Rabalais, J. W. *Principles of U.V. Photoelectron Spectroscopy*; Wiley-Interscience: New York, 1977.

(24) It is important to remind for the following comparison with the theoretical data that the DV-Xα calculations were carried out for models complexes having R = CH_3. Part of the theoretical overestimate of the IEs can be attributed to the less pronounced electron-releasing effect of CH_3 vs C_2H_5.

on switching from the He I to the more energetic He II radiation. The last criterion is particularly useful in the present study since it allows us to discriminate experimentally between ionizations related to MOs with high metal d character and those related to MOs mainly localized on the phoshorus bridging atoms.[25]

$[(CO)_4Cr(\mu\text{-}PR_2)]_2$. The lowest IE band A (Figure 9) is assigned to the ionization from the $7b_{2g}$ π^*(Cr–Cr) MO. The second band B is attributed to four different ionizations: $6b_{1g}$ δ(Cr–Cr), $4a_u$ δ^*(Cr–Cr), $13a_g$ σ(Cr–Cr), and $9b_{3u}$ π(Cr–Cr). All of them, as the $7b_{2g}$ one, have a large localization on the metal centers (over 55%). On the contrary, the bands at higher IEs arise from ionizations of MOs which are mainly localized on the PR_2 bridges, as demonstrated by the very pronounced intensity falloff in the He II spectrum (Figure 9, top). Bands C and D are related to the two Cr–P bonding orbitals ($7b_{3g}$ and $10b_{1u}$, respectively). This assignment is also in tune with the He I relative intensity ratios B:C and B:D, which are roughly 4:1. Band F, with its shoulder E in its lower IE side, is assigned to four P–C bonding orbitals. We propose to assign E to the ionization of the $9b_{2u}$ $P(p_y)$–C bonding MO. Consistently with the expected $9b_{2u}$–$12a_g$ energy separation (experimental, 0.6 eV; theoretical, 0.77 eV), the corresponding in-phase combination ($12a_g$) is taken to be included in band F together with the $8b_{3u}$ and $5b_{1g}$ $P(p_x)$–C bonding orbitals.

$[(CO)_4Mo(\mu\text{-}PR_2)]_2$. As already anticipated in the theoretical section, the PE data of the two isoelectronic Cr and Mo complexes show significant differences that need some discussion (compare Figure 9 and 10).

The lowest IE region contains in both cases four well-resolved bands (A–D), but the relative intensities (A:B:C:D) are changed in the two isoelectronic complexes (Cr, 1:4:1:1; Mo, 1:3:2:1). The theoretical results of Figure 8 contribute to explain the experimental trend. Due to the large destabilization of the $7b_{3g}$ MO (already discussed in the previous section) we observe that the ionization from the $7b_{3g}$ MO moves into the region peculiar to the metal-based MOs describing the metal–metal interactions. The TS procedure (see TSIEs in Table IV) would predict the following assignments: $6b_{1g}$, $4a_u$, and $7b_{3g}$ to band B and $13a_g$ and $9b_{3u}$ to band C. However, the He I/He II intensity changes allow us to correct such assignment to that reported in Table IV. Actually, the assignment of the ionization from $7b_{3g}$ to band C is consistent with the relative intensity decrease of band C vs band B in the He II spectrum.[25]

The change of the profile of band envelope E–F on passing from Cr to Mo is also in tune with the computed reduction of $9b_{2u}$–$12a_g$ (the p_y phosphorus-based orbitals) energy separation. It is likely that in Mo ionizations from $9b_{2u}$–$12a_g$ orbitals contribute both to band E.

$[(CO)_4W(\mu\text{-}PR_2)]_2$. The PE data (Figure 11 and Table IV) are virtually identical with that corresponding to Mo. The minor changes to be outlined are as follows: the 0.23 eV shift toward higher IE of band D and the collapse of bands E and F into one band with two hill-resolved maxima, whose energy separation is ca. 0.3 eV. These differences can be interpreted by assuming a larger stabilization of the $10b_{1u}$ and $9b_{2u}$ MOs as a consequence of the better overlap with the more diffuse metal orbitals.

$[(CO)_4Mn(\mu\text{-}PR_2)]_2$. The first region of the He I spectrum (Figure 12) presents also four bands (A–D), but they are less resolved and suffer a small shift toward higher IE with respect to the previous cases. The assignments are more critical than previously (we have now an extra ionization due to two more electrons), and we propose here only tentative assignments based on the main trends of the theoretical calculations (see Figure 2) and on the experimental evidence that the intensity ratio (A + B + C + D)/(E + F) found in the Cr complex (ca. 1.24) (Figure 9) becomes higher in the Mn complex [(A + B + C + D)/(E) = ca. 1.74] (Figure 12). Both the experimental and theoretical data would suggest that the ionization from the $9b_{2u}$ MO, which was assumed to contribute to the higher IE band E in the previous cases, is now shifted in the first region, contributing to the intensity of band D.

The lowest band A, to be associated with the ionization from the $11b_{1u}$ σ^*(Mn–Mn), has a broader shape than band A of the previous cases. We must remind that in Cr, and the isoelectronic molecules, this band was associated with a π^*(M–M) orbital, so that a different band shape is not surprising.

As expected from the calculations, the Mn–Mn orbitals ($13a_g$, $6b_{1g}$, $9b_{3u}$, $7b_{2g}$, and $4a_u$) span over a very narrow energy range. We propose to assign band B to ionizations from $13a_g$, $6b_{1g}$, $9b_{3u}$, and $7b_{2g}$ MOs and band C to those originating from $4a_u$ and $10b_{1u}$ ones. Band D is then assigned to the $7b_{3g}$ and $9b_{2u}$ components. The large intensity falloff of both band C and band D in the He II spectrum confirms the gross feature of the proposed assignments. Consistently, we take band E to represent three ionizations from $5b_{1g}$, $8b_{3u}$, and $12a_g$ MOs.

Finally, we wish to outline the shift toward lower IE, with respect all previous spectra, of the band labeled as F in Figure 12 to be assigned to ionizations from the carbonyl framework. This effect can be explained by the greater negative charge on the carbonyl framework due to the previously mentioned larger back-donation from Mn atoms.

Conclusions

A very accurate description of the electronic structure of phosphido-bridged dimers has been obtained in the present study. Most of the structural data of the studied series (V, Cr, Mn) have found a consistent explanation in terms of strengthening or weakening of the direct metal–metal interactions, in agreement with previous interpretations.[9,10] However, the present theoretical analysis assigned a remarkable role to the M–bridge interactions. Actually, the large M–M lengthening observed on passing from Cr to Mn is more easily understood if the occupation of a M–bridge antibonding orbital is also taken into account. A careful analysis of the theoretical results furnished also a rationale for the counterintuitive sequence of the occupied σ, π, and δ M–M bonding and antibonding MOs. The role played by the M–bridge interactions appears to be of crucial importance in this case, too.

The UP–PE data provided a consistent energetic picture of the M–M and M–bridge interactions. The spectroscopic data showed distinct changes along the studied V → Cr → Mn series. Small changes between isoelectronic molecules (Cr, Mo, W) have been also detected. The existence of through-space interactions between the phosphorus bridging atoms, maximized in the Mn complex where the P–P distance takes the minimum value, has been fully confirmed by the UV–PE data.

In conclusion, this paper demonstrates the potentiality of the ultraviolet–photoelectron spectroscopy, when coupled to an accurate theoretical method, in obtaining a detailed description of the bonding scheme in transition-

(25) In fact, on the basis of the Gelius model,[26] we expect a marked decrease in the cross-section ratio σ(P 3p)/σ(M *n*d) on passing from the He I to the He II excitation source.

(26) Gelius, U. In *Electron Spectroscopy*; Shirley, D. A., Ed.; North Holland: Amsterdam, 1972; p 311.

metal organometallic complexes.

Acknowledgment. Financial support to this study from Ministero della Pubblica Istruzione (Rome) is gratefully acknowledged.

Registry No. $[(CO)_4V(\mu\text{-}P(CH_3)_2)]_2$, 68365-83-3; $[(CO)_4Cr(\mu\text{-}P(CH_3)_2)]_2$, 19599-74-7; $[(CO)_4Mn(\mu\text{-}P(CH_3)_2)]_2$, 19599-80-5; $[(CO)_4Cr(\mu\text{-}P(C_2H_5)_2)]_2$, 95527-25-6; $[(CO)_4Mo(\mu\text{-}P(C_2H_5)_2)]_2$, 34482-49-0; $[(CO)_4W(\mu\text{-}P(C_2H_5)_2)]_2$, 42830-84-2; $[(CO)_4Mn(\mu\text{-}P(C_2H_5)_2)]_2$, 110551-58-1.

Carbon-13 Monoxide Enrichment of Metal Carbonyl Compounds Employing KH and $NaBH_4$ as Exchange Promoters

Jeffery C. Bricker, Martin W. Payne, and Sheldon G. Shore*

Department of Chemistry, The Ohio State University, Columbus, Ohio 43210

Received April 27, 1987

Carbon-13 monoxide enrichment of the metal carbonyls $Fe(CO)_5$, $M_3(CO)_{12}$ (M = Fe, Ru, Os), $M_2(CO)_{10}$ (M = Mn, Re), and $M(CO)_6$ (M = Cr, Mo, W) at pressures up to 1 atm of ^{13}CO and 25 °C has been examined by using KH and $NaBH_4$ as exchange promoters. With the exception of $Ru_3(CO)_{12}$, it was found that $NaBH_4$ is more effective or at least equal to KH as an exchange promoter and appears to be more useful due to its ease of handling and greater solubility in the solvent tetrahydrofuran.

Introduction

In conjunction with earlier work on the catalysis of the water-gas shift reaction by $[HRu_3(CO)_{11}]^-$[1] we observed that the reaction of KH with triruthenium dodecacarbonyl, $Ru_3(CO)_{12}$, occurred according to the following equilibrium[2] (reaction 1). When a large excess of CO gas was present

$$KH + Ru_3(CO)_{12} \rightleftharpoons K[HRu_3(CO)_{11}] + CO \quad (1)$$

in the system, the forward reaction of reaction 1 was inhibited. When that gas was ^{13}CO, statistical exchange of ^{13}CO–^{12}CO occurred between gas and condensed phases but did not occur when KH was absent.[1a,3] The anion $[HRu_3(CO)_{11}]^-$ readily exchanges bound CO with free ^{13}CO.[1a,5,6] Carbon monoxide exchange is also promoted by $NaBH_4$.[3] More recently,[4] MeO^- was shown to promote ^{13}CO exchange with $Ru_3(CO)_{12}$.

Since utilization of the carbon-13 nuclide as a probe for the characterization and study of organometallic compounds is widespread,[7] a convenient general procedure for enriching metal carbonyls is desirable. Although a variety of methods for ^{13}CO enrichment are known,[4,8] the present report provides a general route that involves mild conditions for enrichment of a variety of carbonyl compounds.

Table I. Carbon-13 Monoxide Enrichment of Metal Carbonyls under 1 atm[a] of ^{13}CO and 0.02 mol % of $NaBH_4$[a] as an Exchange Promoter at 25 °C

expt	metal carbonyl	expt enrichment, %	statistical enrichment, %	time, h
1	$Fe(CO)_5$	69	70	24
2	$Ru_3(CO)_{12}$[b]	54	59	46
3	$Ru_3(CO)_{12}$	16	52	60
4	$Os_3(CO)_{12}$	60	66	24
5	$Fe_3(CO)_{12}$[c]	9	10	8
6	$Mn_2(CO)_{10}$	61	69	24
8	$Re_2(CO)_{10}$	1.1	62	48
9	$Cr(CO)_6$	52	59	24
10	$Mo(CO)_6$	38	50	48
11	$W(CO)_6$	33	55	48

[a] Except where noted. [b] KH used as the exchange promoter. [c] 120 Torr of ^{13}CO.

Scheme I

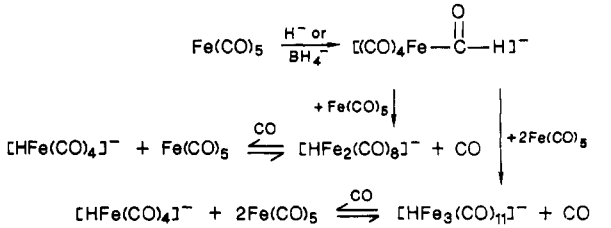

Results and Discussion

Carbon-13 monoxide enrichment of a number of metal carbonyls at pressures up to 1 atm of ^{13}CO and 25 °C has been examined by using KH and $NaBH_4$ as exchange promoters. With the exception of $Ru_3(CO)_{12}$, it was found that $NaBH_4$ is more effective or at least equal to KH as an exchange promoter and appears to be more useful due to its ease of handling and greater solubility in the solvent THF. Table I provides a summary of the most favorable results obtained. Detailed consideration of the systems studied is provided below.

$Fe(CO)_5$. No carbon monoxide exchange between ^{13}CO and $Fe(CO)_5$ was observed over a period of 24 h at 25 °C and 1 atm of ^{13}CO pressure. This is consistent with earlier results.[9] However, when a small amount of KH or $NaBH_4$

(1) (a) Bricker, J. C.; Nagel, C. C.; Shore, S. G. *J. Am. Chem. Soc.* **1982**, *104*, 1444. (b) Bricker, J. C.; Nagel, C. C.; Bhattacharyya, A. A.; Shore, S. G. *Ibid.* **1985**, *107*, 377.

(2) We have shown that the equilibrium is completely reversible, that is, KH and $Ru_3(CO)_{12}$ can be isolated from a THF solution of $K[HRu_3(CO)_{11}]$ that has an atmosphere of CO gas above it (see Experimental Section).

(3) Bricker, J. C. Ph.D. Dissertation, The Ohio State University, Columbus, OH, 1983.

(4) Darensbourg, D. J.; Gray, R. L.; Pala, M. *Organometallics* **1984**, *3*, 1928.

(5) Darensbourg, D. J.; Pala, M.; Waller, J. *Organometallics* **1983**, *2*, 1285.

(6) Payne, M. W.; Leussing, D. L.; Shore, S. G. *J. Am. Chem. Soc.* **1987**, *109*, 617.

(7) (a) Todd, L. J.; Wilkinson, J. R. *J. Organomet. Chem.* **1974**, *77*, 1. (b) Stuntz, G. F.; Shapley, J. R. *J. Am. Chem. Soc.* **1977**, *99*, 607. (c) Darensbourg, D. J.; Salzer, A. *Ibid.* **1978**, *100*, 4119. (d) Darensbourg, D. J.; Baldwin, B. J. *Ibid.* **1979**, *101*, 6447. (e) Geoffroy, G. L. *Acc. Chem. Res.* **1980**, *13*, 469.

(8) (a) Darensbourg, D. J.; Walker, N.; Darensbourg, M. Y. *J. Am. Chem. Soc.* **1980**, *102*, 1213. (b) Darensbourg, D. J.; Darensbourg, M. Y.; Walker, N. *Inorg. Chem.* **1981**, *20*, 1918.

0276-7333/87/2306-2545$01.50/0